Multiple-fibre interferometry setup for probe sample interaction measurements in atomic force microscopy

OPEN ACCESS
IOP Publishing
Measurement Science and Technology
Meas. Sci. Technol. **31** (2020) 094001 (11pp)
https://doi.org/10.1088/1361-6501/ab85d8

Multiple-fibre interferometry setup for probe sample interaction measurements in atomic force microscopy

Petr Klapetek[1,2], Andrew Yacoot[3], Václav Hortvík[1], Václav Duchoň[1], Herve Dongmo[3], Šimon Řeřucha[4], Miroslav Valtr[1,2] and David Nečas[2,5]

[1] Czech Metrology Institute, Okružní 31, 638 00 Brno, Czech Republic
[2] Central European Institute of Technology, Brno University of Technology, Purkyňova 123, 612 00 Brno, Czech Republic
[3] National Physical Laboratory, Hampton Rd, Teddington TW11 0LW, United Kingdom of Great Britain and Northern Ireland
[4] Institute of Scientific Instruments, CAS, Královopolská 147/62, 612 00 Brno, Czech Republic
[5] RG Plasma Technologies, Central European Institute of Technology, Masaryk University, Kamenice 5, 625 00 Brno, Czech Republic

E-mail: pklapetek@cmi.cz

Received 31 December 2019, revised 30 March 2020
Accepted for publication 2 April 2020
Published 16 June 2020

Abstract

Atomic force microscopy (AFM) often relies on the assumption that cantilever bending can be described by simple beam theory and that the displacement of the tip can be evaluated from the cantilever angle. Some more advanced metrological instruments use free-space or fibre interferometers for measuring the position of the cantilever apex directly, thereby simplifying the metrology traceability chain. The next logical development, covering measurements of both the cantilever apex position and its deformation due to lateral forces acting during different AFM measurement regimes, is presented in this paper. It is based on using a set of closely packed fibre interferometers that can be used to determine localised bending of the cantilever at different positions along the cantilever. This can be used for detection of cantilever deformation beyond classical beam theory, and can yield both better understanding of sources of uncertainty in individual AFM force–distance measurements and more accurate scanning in constant height mode in high-speed AFM applications.

Keywords: atomic force microscopy, interferometry, metrology

(Some figures may appear in colour only in the online journal)

1. Introduction

Atomic force microscopy (AFM) is the predominant method used for metrologically traceable measurements of surface topography in the area of nanometrology. A sharp tip on a small cantilever is scanned over the sample surface. The tip is sensitive to small atomic interaction forces (e.g. van der Waals forces) between the probe and sample leading to a deflection of the cantilever. This is normally combined with a feedback loop to keep these forces constant. Traditionally, the detection of cantilever motion is done using an optical lever technique known as beam deflection [1, 3], i.e. by monitoring the changes in position of the laser beam reflected from the cantilever. This is the key principle of the majority of commercial AFMs, and the main benefits of the method are its simplicity and robustness. Although AFM manufacturers have considered using optical interferometry, it is bulkier [1, 4]. However, the sensitivity of an optical interferometer can be higher and has the advantage of traceability [5]. From a metrology point of view,

the optical lever technique has many disadvantages, since it does not measure the cantilever displacement, but only the local angular deflection of the cantilever. The motion of the cantilever can be therefore monitored only as a derived quantity, based on many different assumptions or experimental calibration. If the cantilever deflection is kept constant during the microscope operation, the problem almost vanishes. However, if the cantilever displacement is used for any measurement, as in the cases of force–distance curve acquisition or contact-mode high-speed imaging, the uncertainty associated with the optical lever pickup method is too high.

As an alternative to both bulk optical interferometry and beam deflection, fibre interferometry can be used for monitoring cantilever displacement. This has been done in the past, e.g. for more accurate probe–sample interaction monitoring purposes [6] or for more accurate measurements in liquid conditions [7]. Despite different attempts to simplify the adjustment of the cantilever and fibre, e.g. by further integration of the cantilever with the fibre by manufacturing it from the fibre [8, 9], the method is still significantly harder to operate than the optical lever technique and often the ferrule associated with the fibre makes viewing of the sample optically more difficult. The technique is therefore less attractive as a source of feedback in AFM imaging.

There are at least two classes of problems where fibre interferometry could significantly reduce the measurement uncertainties. First, with the advent of novel nanomechanical regimes (like PeakForceQNM by Bruker), the use of force–distance data for quantitative measurements has grown massively. The AFM probe/cantilever assembly is, however, not an ideal tool for performing nanoindentation experiments. It is mounted at an angle with respect to the surface normal and when it is pressed towards the surface, there is a lateral force acting on the cantilever, for which a compensation must be made [10]. This is not always done and in principle the cantilever bending can lead to either the probe slipping on the surface during indentation or to the probe apex sticking to the surface, causing additional and more complex cantilever bending due to restriction of motion. By using the optical lever technique any systematic errors caused by the change in shape of the cantilever are magnified. In contrast to this, although a single-fibre interferometer cannot resolve the true cantilever shape, it can detect the real position of the probe more accurately than a beam deflection detection system as it does not rely on cantilever bending.

Secondly, an accurate measure of the cantilever displacement is needed for open-loop contact-mode high-speed imaging. In this family of techniques the probe is used as a height sensor, travelling very fast over the surface, surpassing the speed limitations of all conventional approaches [11]. The cantilever surfs above the surface and deflects by an amount corresponding to the surface topography since there is no closed loop correction [12]. From a metrology point of view, this approach is limited by the presence of different ringing artefacts related to cantilever vibration excitation when scanning across topographical features [13]. Here, a displacement measurement instead of cantilever deflection is a way to measure and reduce the effects of such artefacts by measuring the displacement of the cantilever at a position on the cantilever where the ringing effect is not present, as was demonstrated with the use of laser Doppler vibrometry [14]. However, a laser vibrometer is a large, expensive device unsuitable for a typical AFM measurement setup.

Previous work by Dorozhovets *et al* [15] has demonstrated simultaneous measurement of cantilever deflection and displacement. In this paper we measure cantilever deflection using a multi-fibre interferometer setup. Unlike previous work, with this setup using multiple-fibre interferometers it is possible to measure both the cantilever displacement at the end of the cantilever and deformation at other positions on the cantilever. This can be used for quasi-static experiments such as nanoindentation with AFM and for dynamic experiments such as high-speed imaging. Compared with laser Doppler vibrometry, the setup is much simpler, less expensive and can provide information about cantilever shape changes during AFM operation. This includes both the cantilever deformation related to static deflection while scanning in the passive high-speed regime, and the dynamic response to topography like the above-mentioned ringing artefacts.

2. Experimental arrangement

In order to measure the cantilever displacement at multiple locations, we constructed a fibre interferometer head with three independent closely packed interferometers. The design of the interferometer is based on work described by Rugar [16] and adapted for metrology in reference [6]. CAD drawings of the mechanical setup are shown in figures 1(A) and (B), and 1(C) shows a photograph of the fibres above the cantilever. The key part of the setup are the fibres that were etched in order to reduce their diameters, typically from 80 μm to 25 μm, and then glued together and attached to an adjustable fibre holder in the head. The fibre ends were then polished. During the polishing process, the presence of interference is tested using a cantilever or a mirror on an actuator, to ensure that the fibres are flat enough. The cantilever was mounted in a PointProbe Plus alignment chip from Nanosensors, which can be used for repeatable mounting of cantilevers without the need for further adjustment. The whole cantilever/alignment chip setup was then aligned so that it was centred above the fibres (with the help of manual adjusters and an optical microscope) at a height of approximately 10 μm above the fibres. Further motion was performed using a piezoelectric actuator that was capable of moving the fibres with respect to the rest of the head by 15 μm. Moreover, the cantilever/alignment chip assembly was located on another smaller piezoelectric actuator for cantilever oscillations in non-contact-mode measurements (that are not performed in this paper). Figure 2 shows the optical arrangement of the fibre interferometers. Light from a stabilised helium neon laser passed through an optical isolator that prevented light from being reflected back into the laser. The light was coupled into a 1×4 fibre splitter. Only three of the splitter outputs were used; they were coupled into three separate 2×2, 50:50 fibre couplers, one for each interferometer. Detectors R_1, R_2 and R_3 recorded 50% of the input

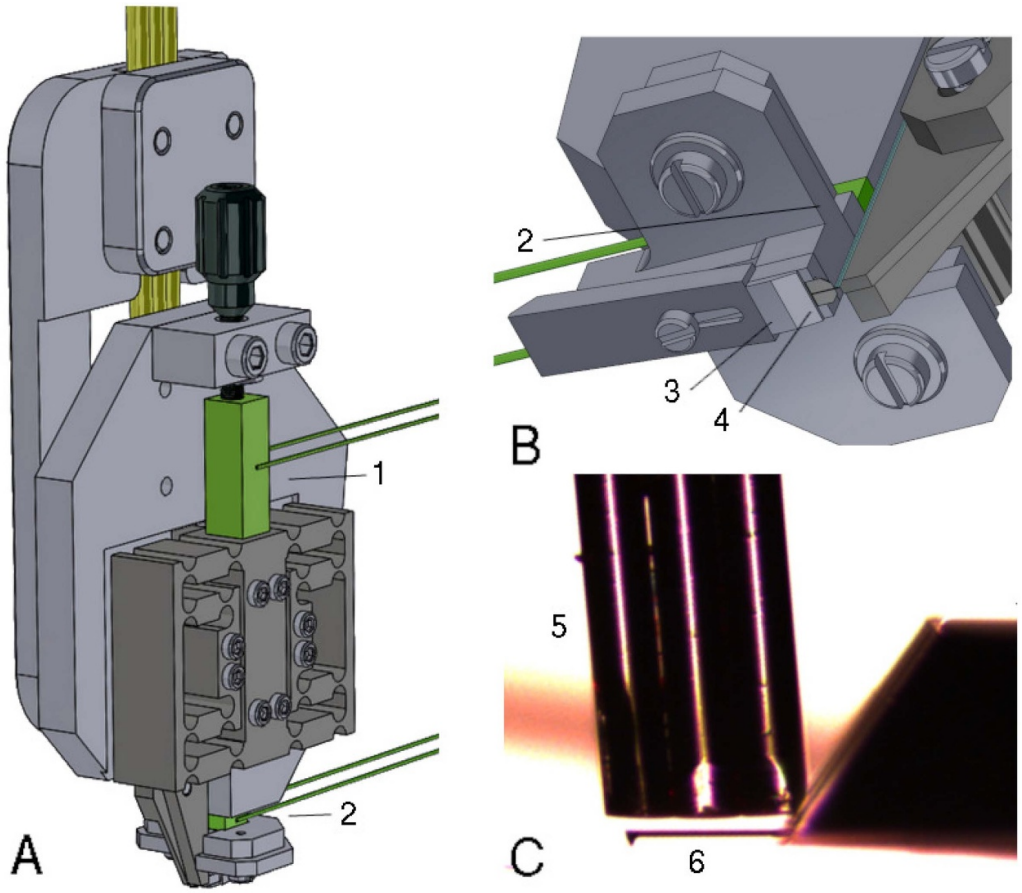

Figure 1. Fibre head schematics: (A) rear view showing the head movement mechanism (1) and fibre movement mechanism (2); (B) front detail showing the fibres and cantilever adjustment, mounting (3) and spring mechanism (4); (C) optical photograph of the fibres (5) and cantilever (6) area.

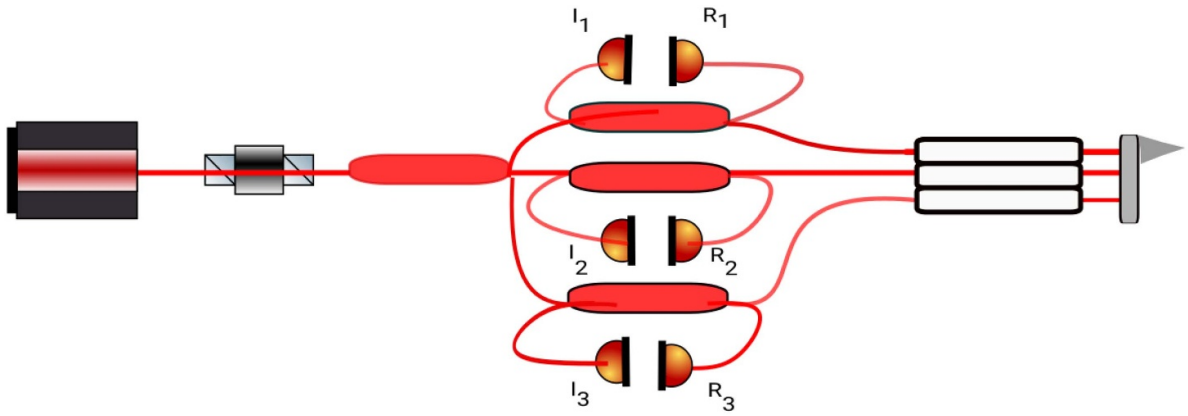

Figure 2. Optical schematics of the system showing, from the left, the laser, an optical isolator, the fibre splitter and light coupled into the three fibre interferometers. The detectors $I_{1,2,3}$ receive the interference signals and the detectors $R_{1,2,3}$ receive the reference signals.

signal, and in each of the three interferometers this signal was used to normalise the interferometer signal for variations in the intensity of the laser beam. The other 50% of the light was transmitted though the other exit port of the fibre that was above the cantilever. About 4% of that light was reflected back from the exit face of the fibre back into the coupler and onto detector I_n, where n represents the interferometer number. The remaining light exited the fibre, diverged and was incident onto the cantilever. Given that the numerical aperture of the fibre was nominally 0.12, the mode field diameter of the fibre was 4.5 μm and the fibre–cantilever separation was approximately 10 μm, the size of the spot on the cantilever was under 20 μm in diameter, considerably less than the 40 μm cantilever width. This light was reflected back towards the fibre and some of it

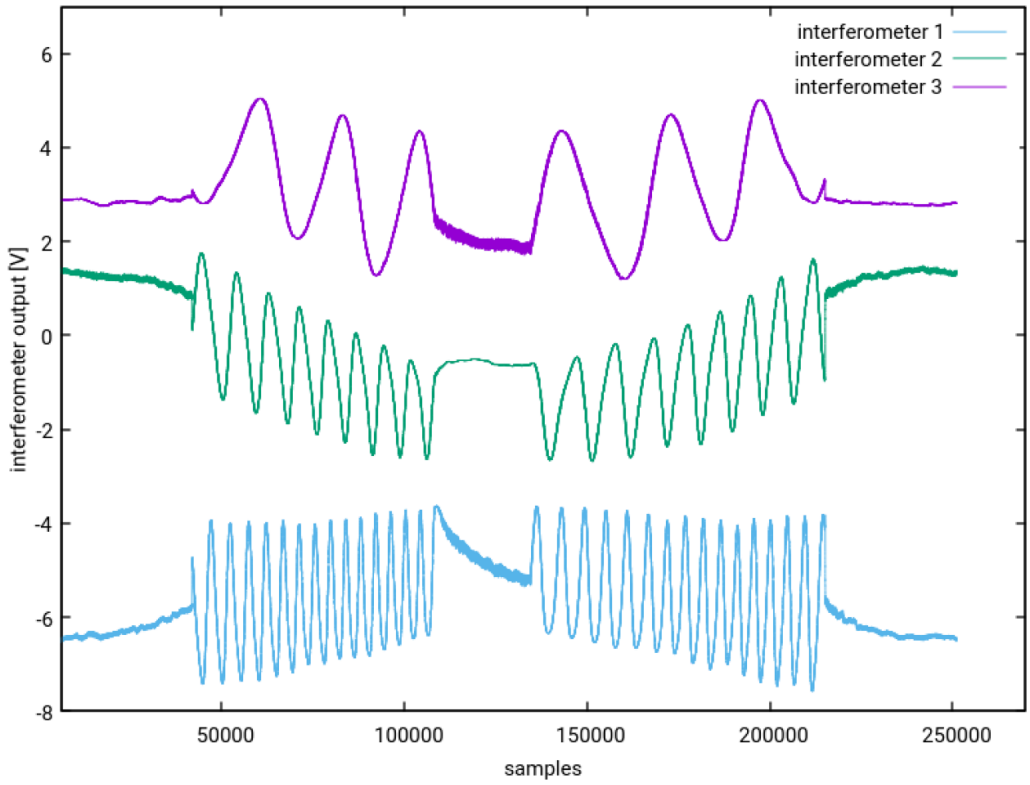

Figure 3. Signal from the three interferometers while the cantilever is pressed towards the surface and released.

was re-coupled back into the fibre. It interfered with the light reflected from the back surface of the fibre. This interference signal was measured by the I_n detector.

Unlike a conventional displacement interferometer, there is an exponential DC offset on the interference signal and a corresponding decrease in fringe contrast with increasing cantilever–fibre separation [17]. To evaluate the signals we use electronics developed at the National Physical Laboratory. Pig-tailed photodiodes were attached to two separate ports of each of the 2×2 fibre couplers. The electronics for each interferometer comprised two transimpedance amplifiers, one for each photodiode. The signal from the reference channel was used to subtract the DC offset from the interference signal. This ensured that the fibre interferometer signal could be amplified with no DC offset and hence the full dynamic range of the data acquisition card (± 5 V) could be used. Data were collected by a simultaneous sampling data acquisition card (NI PCI 6143) together with signals from all the piezoelectric actuators in the system.

A typical set of signals coming from all three interferometers during force–distance data acquisition using the AFM is shown in figure 3. All interferometers measure over a few fringes in one direction during the approach part of the curve, and in the other direction in the withdrawal part of the curve. It can be also seen that the amplitudes and positions of fringe maxima and minima slightly change due to cantilever bending. This is an effect that is not observed if a fibre interferometer is used only for a small bending detection (as in a typical servo control application); however, it must be taken into account in the case of force–distance curve measurements where the bending of the cantilever is larger. The steady part of the indentation curve, when the cantilever is pressed maximally and should not move, can be used to illustrate the need for more advanced data processing. On interferometer 1 (close to the rear of the cantilever) we can see that even if there should be no motion, there is still some drift related to use of the open-loop piezo actuator for indentation. Similar drift can be seen in the signal from interferometer 3 (close to the cantilever base), but much smaller and already hiding in the noise as the motion of the cantilever at this position is significantly smaller. However, the signal of interferometer 2 is around the interferometer output maximum at this moment and therefore we cannot distinguish the motion direction. An acquisition and data processing method that would be sensitive to motion direction is therefore needed even for a simple experiment like force–distance curve measurement.

3. Data acquisition and processing

The simple Michelson fibre interferometer used here provides only phase information as there is only one interference signal; many displacement interferometers have two signals in phase quadrature, in order to provide information about the direction of motion. Normally when this simplest type of fibre interferometer is used for detection of cantilever motion it is combined with a servo control system that acts as a null

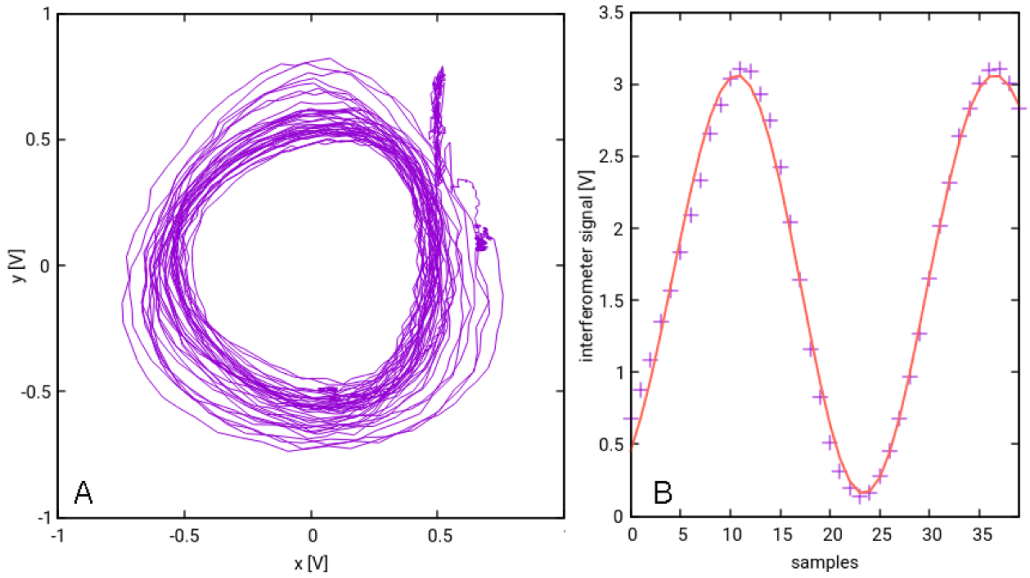

Figure 4. Demodulation methods principle and operation: (A) small amplitude dithering sine and cosine output after synchronous demodulation and Heydemann correction; (B) large amplitude dithering fit on an individual linearised part of the interference signal obtained from large amplitude modulation—a similar part of a sine function is obtained for every dithering cycle in the fitting-based demodulation method.

sensor based on a constant height (in contact mode) or amplitude of oscillation (in the non-contact case). In this case the displacement is limited to within just less than half of a fringe centred on the approximately linear region of the fringe between a maximum and minimum. The direction of motion can then be determined by the change in displacement signal. This limited range is, however, not suitable for force–distance curve acquisition, which often requires displacement to be measured over a larger range. In this case, we encounter the fringe maxima and minima from which we cannot determine if the motion continued in the same direction or if the direction was reversed. From looking at the graphs in figure 3 and knowing that the direction changed, the point at which the direction changed can be deduced; however, this situation is not ideal and some method of determining the direction of motion purely from the interferometer signals is necessary.

Fortunately, in our setup, the three fibre interferometers are slightly phase-shifted with respect to each other (due to imperfections in the fibre ends, polishing and the fibre–cantilever tilt adjustment). This means that when the whole cantilever was moved in the same direction, we could use the information from interferometers that were not at the maximum or minimum of the fringe to reconstruct the motion direction for the interferometer signal that was at a fringe maximum or minimum. This method worked only when we were able to normalize the interferometer signals appropriately within the range of ± 1. As can be seen from figure 3, the amplitudes of the maxima and minima change as a function of position so, for normalization, data needs to be collected over a range that includes several maxima and minima. Due to this constraint, the method is also unsuitable for real-time operation as the whole signal needs to be processed at once. We also need to have the maxima and minima available for the normalization, so the method is suitable only when a large motion is measured. On the other hand, real-time evaluation is useful in order to fully employ the sampling speed (250 kHz) of the data acquisition card, as there is no data loss due to data processing and modulation/demodulation.

As an alternative, we can get the phase information in a more robust and universal way by dithering the length of the measurement arm of the interferometer and applying a demodulation of the interferometer signal. If we are periodically moving (dithering) the measurement arm (distance between fibre ends and cantilever) faster than the speed at which the AFM cantilever deflects in normal operation, we can use the knowledge of the instantaneous direction of motion caused by dithering to detect the direction of the slower motion of the cantilever.

The dithering amplitude and frequency can vary widely and different approaches can be used to get the direction information in the data processing phase. If a small amplitude is used for dithering, e.g. a tenth of the fringe (approx. 30 nm), the data can be demodulated using the *synchronous demodulation* approach presented in reference [18] based on multiplication of the interferometer output by the dithering signal and performing a time average over the dithering period (in order to generate the 'cosine' signal). When combined with the time average of the signal itself (providing the 'sine' component), both necessary signals for conventional quadrature detection are obtained. This can be further improved by the usual data processing approach for (quadrature) sine and cosine signals, which is the Heydemann correction [19] as applied by Birch [20] for removing ellipticity in the Lissajous signal formed by combination of imperfect sine and cosine signals. The main disadvantage of this method is that it is more sensitive to

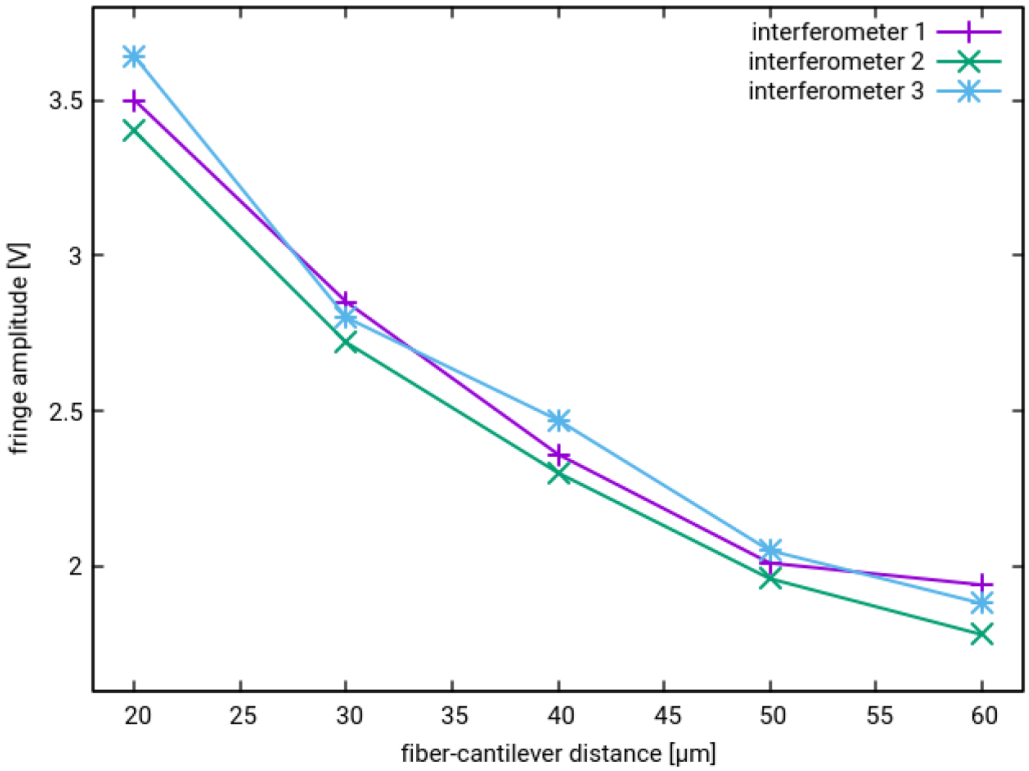

Figure 5. Fringe amplitude dependence on fibre–cantilever distance.

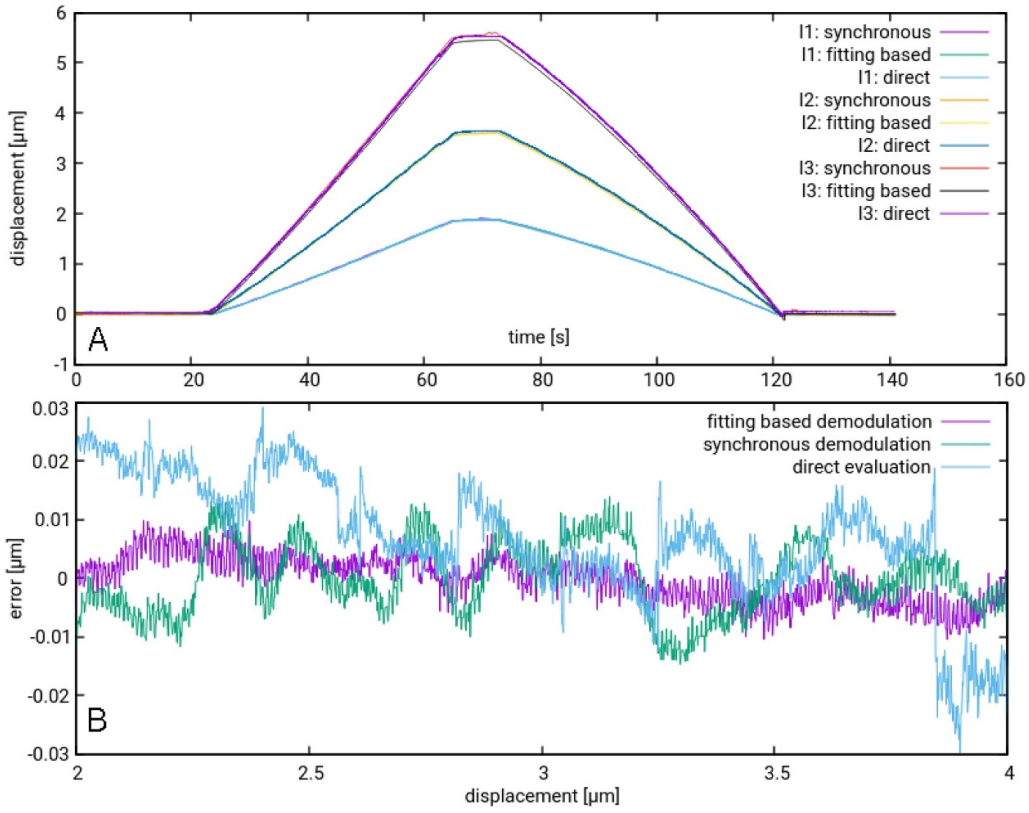

Figure 6. Comparison of demodulation methods on a single indentation into a sapphire sample: (A) overall shape of the cantilever displacement during force–distance curve acquisition evaluated by the three methods and for the three interferometers (I_1, I_2 and I_3); (B) errors of the individual curves from the ideal shape during the loading part of the curve for one of the interferometers.

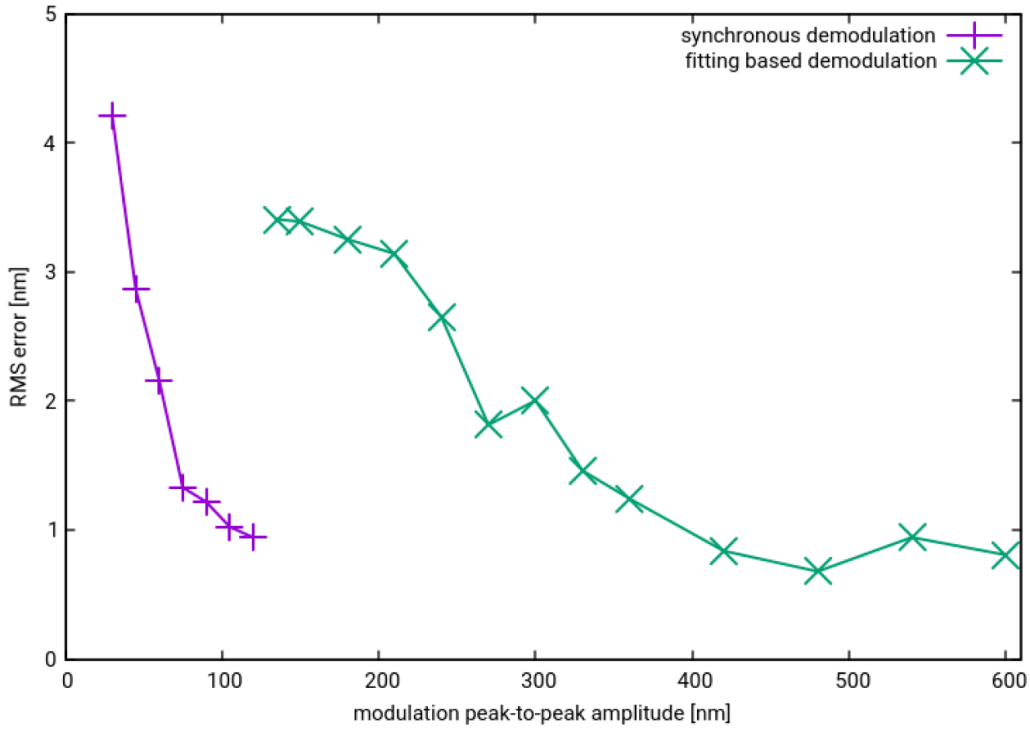

Figure 7. Demodulation error evaluated for different modulation amplitudes and both data processing methods.

signal noise, both due to the smaller dithering amplitude and the multiplication of signals that might have the same noise source superimposed on them (e.g. 50 Hz multiples), which is then significantly amplified. Moreover, when the motion is small, there might not be enough data for performing the Heydemann correction for which a displacement of at least one optical fringe, i.e. 316 nm, is required. An example of the sine/cosine signals detected by this demodulation method for a single force–distance curve measurement is shown in figure 4(A). It is clear to see that although the Heydemann correction has been applied, the Lissajous signal is still far from a perfect circle. We believe that this non-ideal shape is related to the presence of multiple reflections between the fibre end and the cantilever. In the fibre interferometer setups normally used for AFMs, the fibre is simply cleaved and uncoated so is only weakly reflective. However, in our case, the fibre ends were polished making them slightly more reflective. As such there was a greater chance of multiple reflections between the cantilever and the end of the fibre. These are insufficient to form a proper Fabry–Perot cavity as in the case of reference [2], where the end of the fibre was partially coated. However, the partial reflections would have been strong enough to cause non-linearity in the optical interferometer. In addition, the amplitude of the signals changes due to the bending of cantilever as demonstrated in figure 3. The latter will cause some 'breathing' of the Lissaujous, resulting in a variation of the radius of the circle.

As an alternative to the above method, the interferometer signal can be dithered with a signal with an amplitude greater than a fringe. The correct phase was estimated by fitting a sine function to the data; therefore, for the rest of the paper we call the method *fitting-based demodulation*. To implement this method, the following steps were necessary.

(a) The signal representing voltage applied to the dithering actuator was segmented into individual periods; each of the following steps was then applied during each of the periods.
(b) An array of x values was obtained by linearising the sine dependence of the dithering piezo motion.
(c) An array of y values was obtained from the interferometer signal values.
(d) A sine function was fitted to this linearised signal (see figure 4(B)), and the amplitude and phase were extracted and stored. The phase obtained in the previous period was used as the initial parameter for fitting, thereby ensuring continuity.
(e) The detected phase was used to determine the motion of the interferometer arm and the amplitude of the signal was used for monitoring variations in the fringe contrast (similarly to the radius of the sine/cosine plot in the synchronous demodulation method).

The advantage of this method was that it could easily handle situations where the contrast of the fringes changed with displacement, and was less sensitive to noise as this was eliminated in the fitting process. However, it needed much larger dithering amplitudes which created the risk of generating some unwanted mechanical vibrations in the AFM head. In practice, the modulation frequencies were between 15 Hz and

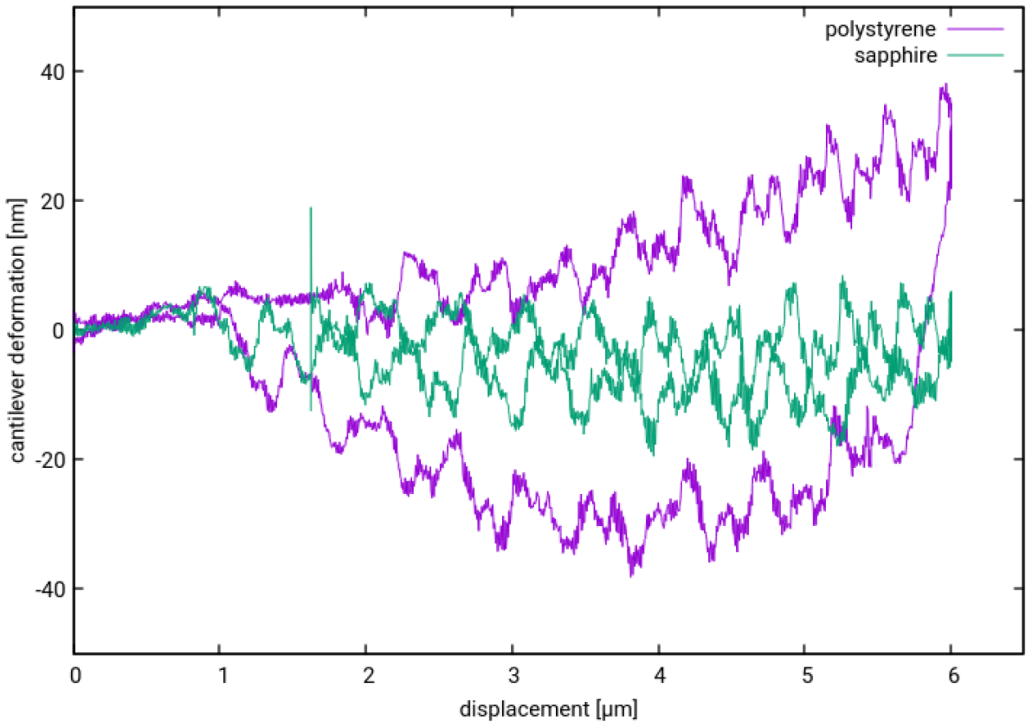

Figure 8. Cantilever deformation out of classic beam theory during indentation on a polystyrene and sapphire substrate.

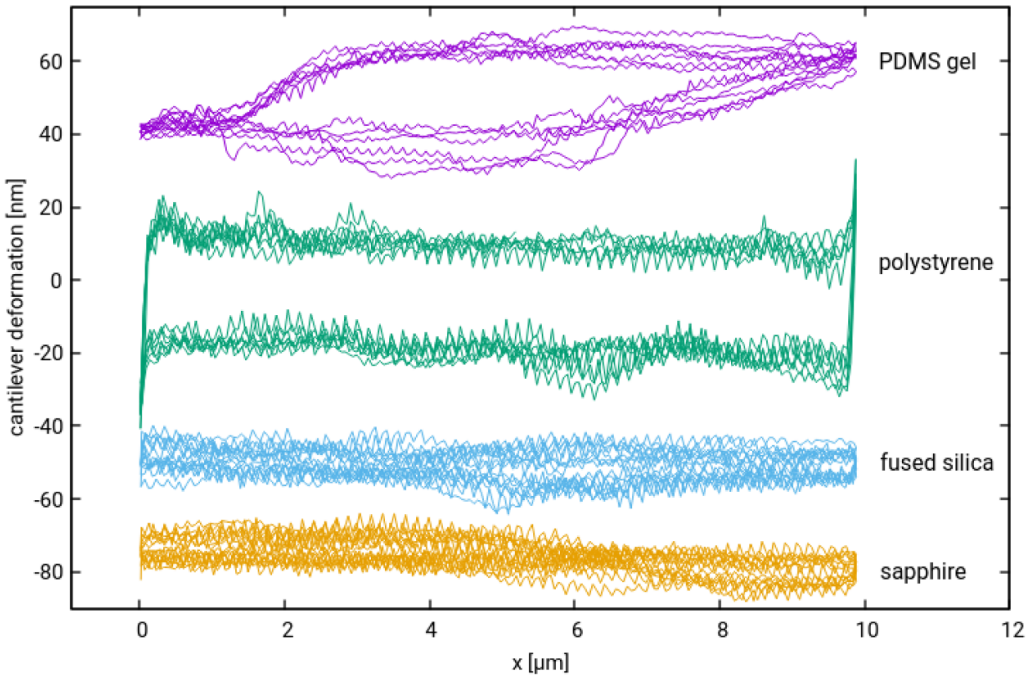

Figure 9. Cantilever deformation out of classic beam theory during scanning of the flat reference samples; a few repeated scan lines are shown together. Data are shifted vertically for better visibility.

2 kHz for different experiments and the speed of the above data processing via fitting was approximately 2000 fittings per second, so for frequencies up to 2 kHz the calculation could be performed in real time.

All the three data processing methods provide the same output: a time-dependent measure of fibre–cantilever separation. As the same procedures were used to process data from all three fibres, simultaneous values of the fibre–cantilever distance in three different locations were obtained, which were then used for analysis of the instantaneous cantilever deformation. All methods of interferometer signal processing are compared in the next section.

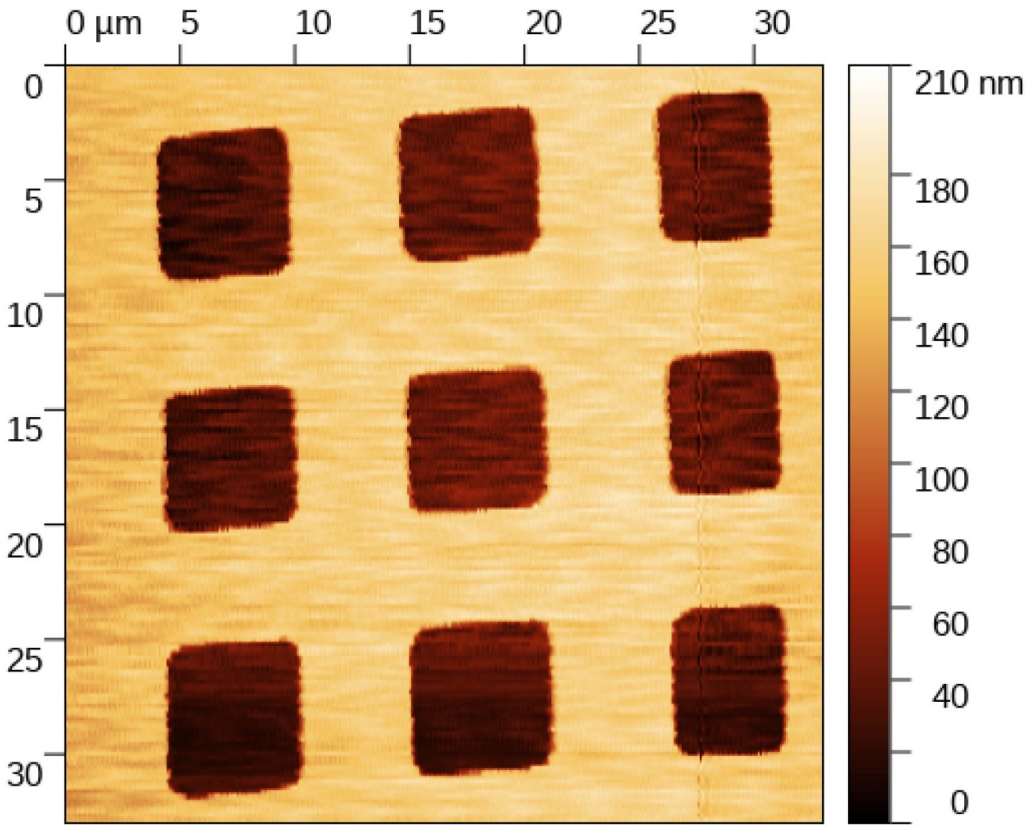

Figure 10. Scan in the passive regime, using no feedback loop for the cantilever and monitoring only its displacement. The lateral deformation comes from the open-loop scan stage used for test purposes.

From the Euler–Bernoulli beam theory we can estimate the beam deflection at any arbitrary point along the x-axis (oriented along the length of the cantilever) as

$$z_x = \frac{Fx^2}{6EI}(3L - x) \tag{1}$$

where the area moment of inertia $I = (wt^3)/12$, E is the elastic modulus, L is the cantilever length, F is the acting force, and w and t are the width and thickness of the cantilever, respectively. The above equation can be used for two purposes. First, when we expect that there should not be any unwanted lateral cantilever motion restriction due to the tip sticking to the substrate (e.g. when small forces are applied on hard surfaces), we can use it to determine the positions of the light spots on the cantilever, by searching for the positions of best fit. The light spot location could also be evaluated on the basis of the images from the optical microscope; however, this would provide only diffraction-limited accuracy. Moreover, the fibres might be slightly misaligned from the cantilever normal direction, so for different fibre–cantilever separations the real spot positions might be systematically shifted. Fitting the ideal spot position from the small bending data gives variance of around 100 nm, which, corresponding to the expected bending angles, leads to about 6 nm uncertainty for the maximum bending of 7 µm shown in this paper. This is clearly a dominant uncertainty component for the system. The other important uncertainty source is the data processing, addressed in the next section, and the electronics- and vibration-related noise, which is approximately 1 nm.

4. Results and discussion

To estimate the range of fibre–cantilever spacing in which the system can operate, we have measured the dependence of the fringe amplitude on the separation distance. The amplitude was determined by dithering the fibre position by 1 µm and frequency by 1 Hz. The fibre–cantilever separation was estimated using an image obtained from an optical microscope. As can be seen from figure 5, within the available manual adjustment range, the signal is decaying approximately exponentially; however, even with a fibre–cantilever spacing as large as 60 µm the interferometer is operational since the size of the light spots on the cantilever are still smaller than the cantilever width. For comparison, the PPP-NCLR cantilever nominal width is 38 µm. The adjustment of the fibre–cantilever separation is therefore not a critical part of the probe mounting and, when using the alignment chip, the probe mounting complexity is not significantly higher than for a usual commercial AFM.

To compare the three possible interferometer signal processing methods, a set of indentations were made into a sapphire sample, using a soft PPP-CONTR cantilever (stiffness 0.2 N m^{-1}). Ideally, we should observe only cantilever bending in this case, as sapphire is much stiffer than the

cantilever-tip system. The experiments were run with the same probe, i.e. preserving the same settings and positions of the fibre interferometers and also indentation on the same spot on the sample (as we expect that there should be no sample deformation in this case). The results are shown in figure 6, together with the errors of the individual methods. These errors were obtained by comparison with an average curve obtained from another set of indentations, evaluated by fitting-based demodulation, which was found to be most accurate across all the experiments. The direct method seems to be the least accurate due to imperfect identification of the fringe maxima and minima in the noisy signal. However, this method is the fastest. Although speed is not critical for indentations, it is important for scanning applications.

In a similar experiment we tested the range of dithering amplitudes suitable for different demodulation methods. A set of simple force–distance curves with different modulation settings was acquired by pressing the same soft cantilever to a sapphire substrate. A set of three curves were measured for each modulation amplitude and both methods were used to evaluate the data. The mean square values of the errors evaluated for different modulation amplitudes and demodulation methods are shown in figure 7. The presented data come only from the valid curves, i.e. from cases when the demodulation yielded a result free of jumps between consecutive interference fringes. We can see that around the peak-to-peak amplitude of 130 nm, i.e. an optical path difference trajectory of somewhat less than half a fringe, there is a region where simple synchronous demodulation starts to fail and the fitting methods becomes usable. It can be also seen that the fitting method can produce results that are about 30% more accurate (0.68 nm vs 0.92 nm RMS error for the best cases); however, with careful choice of displacement amplitude, the accuracy of both methods is sufficiently high for cantilever displacement measurements. The limit of the methods is related to the imperfect shape of the fringes, which has an impact both on the synchronous demodulation (as the Heydemann correction cannot compensate for all deviations from circularity; see also figure 4(A)) and on the fitting (as the shape of the modulated signal is not an exact sine function; see also figure 4(B)). Using some more advanced models of the fringe could help in both cases; however, this is a parameter that would need to be tuned for each cantilever independently. The present accuracy in the nanometre range is already suitable for many experiments.

An example of how the cantilever deforms in practice compared to the beam theory is shown in figure 8, obtained for indentation into a polystyrene thin film sample from Bruker. The cantilever deformation was evaluated as the difference between the displacement measured by the interferometer at the centre of the cantilever and the ideal displacement evaluated from beam theory. As a reference for applying beam theory, the displacement measured at the cantilever apex was used. The hysteresis loop shows the impact of friction and sticking of the probe apex during the indentation. As the probe can not slide freely across the surface, it deforms; the direction of this deformation is dependent on the direction of the motion during indentation and the magnitude of the deformation depends on the surface material under investigation. This leads to a systematic error when the cantilever displacement is evaluated using a standard beam deflection method.

In figure 9 the effect of friction and tip sticking is studied more systematically. The tip is scanned in the cantilever orientation direction; a single line scan took 25 s and cantilever deformation out of classical beam theory was evaluated for different materials (PDMS gel, polystyrene thin film, fused silica and sapphire, all from the Bruker PeakForceQNM test sample set) with the same contact force (approximately 300 nN, evaluated from the deflection during approach and nominal cantilever stiffness). A few scans are shown to demonstrate the reproducibility of the results. It can be seen that both the magnitude and shape of the deformation hysteresis curves depend on the visco-elastic properties of the used material. This cantilever deformation would lead to a systematic difference in the forward and reverse scan lines if a standard beam deflection method were used, which is also often observed on commercial instruments when the fast axis is oriented along the cantilever axis.

Finally, we demonstrate the ability of the multiple-fibre head to be used for AFM imaging. The used data acquisition card with a 250 kHz sampling rate is not fast enough for real high-speed AFM imaging; however, the presented example of a constant-height scan (see figure 10) was made using the same passive scanning regime as in our high-speed system [21], so the high-speed scanning and cantilever deformation detection should be possible using a faster data acquisition card in future. It was also scanned in the same way, storing raw data and positions in a general *xyz* format [22] and processed using Gwyddion open-source software [23]. The replacement of the data acquisition card by a high-speed one should therefore be straightforward. Note that the scan was performed using a low-cost open-loop positioning table and an open-loop piezo amplifier (both from Thorlabs), so the lateral scale is distorted by the positioning table non-linearity and hysteresis.

5. Conclusions

A method for atomic force microscopy cantilever displacement and deformation measurements using a set of fibre interferometers is presented. The method can be used for detecting the parasitic cantilever deformation during force–distance curve data acquisition or for replacing a laser Doppler vibrometer in high-speed AFM imaging. Even if the manufacturing complexity is higher than for a standard laser deflection method, the operation itself (e.g. the probe exchange) is only slightly more complex and the amount of added information in this measurement setup is high. The capability of measuring impact of lateral forces on cantilever static and dynamic behaviour in real time opens novel possibilities of reducing the uncertainty components of AFM imaging, both in nanomechanical measurements and in high-speed imaging.

Acknowledgments

The research leading to these results has received funding from the European Metrology Programme of Innovation and

Research project 3D Nano, from project OP-PIK Grant No. CZ.01.1.02/0.0/0.0/15_019/0004 676 and project CEITEC 2020 under Grant No. LQ1601. In addition funding was received from the Engineering Measurement programme of the National Measurement System UK.

ORCID iDs

Petr Klapetek https://orcid.org/0000-0001-5241-9178
Andrew Yacoot https://orcid.org/0000-0001-6740-821X
Šimon Řeřucha https://orcid.org/0000-0002-2026-5159
Miroslav Valtr https://orcid.org/0000-0002-7628-9184
David Nečas https://orcid.org/0000-0001-7731-8453

References

[1] Putman C A J, de Grooth B G, van Hulst N and Greve G J 1992b A detailed analysis of the optical beam deflection technique for use in atomic force microscopy *J. Appl. Phys.* **72** 62
[2] Oral A, Grimble R A, Özer H O and Pethica J B 2003 High-sensitivity noncontact atomic force microscope/scanning tunneling microscope (nc AFM/STM) operating at subangstrom oscillation amplitudes for atomic resolution imaging and force spectroscopy *Rev. Sci. Inst.* **74** 3656
[3] Putman C A J, de Grooth B G, van Hulst N and Greve G J 1992 A theoretical comparison between interferometric and optical beam deflection technique for the measurement of cantilever displacement in AFM *Ultramicroscopy* **42–44** 1509–13
[4] Beaulieu L Y, Godin M, Laroche O, Tabard-Cross V and Grütter P 2007 A complete analysis of the laser beam deflection systems used in cantilever based systems *Ultramicroscopy* **107** 422–30
[5] Vorbringer-Dorozhovets N, Mastylo R and Manske E 2018 Investigation of position detectors for atomic force microscopes *Meas. Sci. Technol.* **29** 105101
[6] Yacoot A, Koenders L and Wolff H 2007 An atomic force microscope for the study of the effects of tip–sample interactions on dimensional metrology *Meas. Sci. Technol.* **18** 350
[7] Rasool H I, Wilkinson P R, Stieg A Z and Gimzewski J K 2010 A low noise all-fiber interferometer for high resolution frequency modulated atomic force microscopy imaging in liquids *Rev. Sci. Instr.* **81** 023703
[8] Iannuzzi D 2006 Monolithic fiber-top sensor for critical environments and standard applications *Appl. Phys. Lett.* **88** 053501
[9] Chang P I, Chavan C, Paris D R and Iannuzzi Schitter D G 2013 Towards high speed ferrule-top atomic force microscopy *IFAC Proc. Volumes* vol **46** pp 131–7
[10] Huang L, Meyer C and Prater C 2007 Eliminating Lateral Forces During AFM Indentation *J. Phys.: Conf. Ser.* **61** 805
[11] Brown B P, Picco L, Miles M J and Faul C F J 2013 Opportunities in high-speed atomic force microscopy *Small* **9** 3201–11
[12] Heaps E, Yacoot A, Dongmo H, Picco L, Payton O D, Russell-Pavier F S and Klapetek P 2020 Bringing real-time traceability to high-speed atomic force microscopy *Meas. Sci. Technol.* in print (https://doi.org/10.1088/1361-6501/ab7ca9)
[13] Klapetek P, Picco L, Payton O D, Yacoot A and Miles M J 2013 Error mapping of high-speed AFM systems *Meas. Sci. Technol.* **24** 025006
[14] Payton O D, Picco L, Robert D, Raman A, Homer M E, Champneys A R and Miles M J 2012 High-speed atomic force microscopy in slow motion–understanding cantilever behaviour at high scan velocities *Nanotechnology* **23** 205704
[15] Dorozhovets N, Hausotte T, Hofmann N, Manske E and Jäger G 2006 Development of the interferometrical scanning probe microscope *Proc. SPIE* **6293** 629311
[16] Rugar D, Mamnin H J and Guenther P 1989 Improved fibre optic interferometer for atomic force microscopy *Appl. Phys. Lett.* **55** 2588–90
[17] Murphy K A, Gunther M F, Vengsarker A M and Claus R O 1991 Quadrature phase shifted, extrinsic Fabry–Perot optical fiber sensors *J. Opt. Soc. Am.* **16** 273–5
[18] Řeřucha Š, Buchta Z, Šarbort M, Lazar J and Číp O 2012 Detection of interference phase by digital computation of quadrature signals in Homodyne laser interferometry *Sensors* **12** 14095–112
[19] Heydemann P L M 1981 Determination and correction of quadrature fringe measurement errors in interferometers *Appl. Opt.* **20** 3382–4
[20] Birch K P 1990 Optical fringe division with nanometric accuracy *Prec. Eng.* **12** 195–8
[21] Klapetek P, Valtr M, Picco L, Payton O D, Martinek J Yacoot A and Miles M J 2015 Large area high-speed metrology SPM system *Nanotechnology* **26** 065501
[22] Klapetek P, Yacoot A, Grolich P, Valtr M and Nečas D 2017 Gwyscan: a library to support non-equidistant scanning probe microscope measurements *Meas. Sci. Technol.* **28** 034015
[23] Nečas D and Klapetek P 2012 Gwyddion: an open-source software for SPM data analysis *Cent. Eur. J. Phys.* **10** 181–8